A level-set approach to large eddy simulation of premixed turbulent combustion

By L. Duchamp de Lageneste AND H. Pitsch

1. Motivation and objectives

Large eddy simulation (LES) of premixed turbulent combustion is now considered to be a promising field. It has the potential to improve predictions of reacting flows over classical Reynolds-averaged Navier-Stokes (RANS) approaches.

Since the reaction zone thickness of premixed flames in technical devices is usually much smaller than the LES grid spacing, chemical reactions occur completely on the sub-grid scales and hence have to be modeled entirely. There are several ways to treat the problem.

One approach by Veynante *et al.* (1997) and Colin *et al.* (2000) is to thicken the flame by artificially increasing the diffusivity to be able to resolve the flame on the LES grid. In order to correct the effect on the flame propagation speed, the chemical source term has to be modified by the use of efficiency functions obtained from direct numerical simulations (DNS) (Angelberger *et al.* (2000)). The main drawback of this method is that it changes the principle underlying physical process from a transport controlled to a chemistry controlled combustion mode.

Chakravarthy *et al.* (2000) have suggested a method in which the scalar processes that can be resolved spatially and temporally are simulated on a 3D LES grid while small scales and faster subgrid combustion processes within each LES cell are simulated using the one dimensional Linear Eddy Model (LEM). This multiple scale approach, can lead to a significant increase in the complexity of the code due to the introduction of a Lagrangian volume-of-fluid (VOF) transport scheme used to track the flame in each cell and due to the definition of a grid-subgrid coupling procedure.

Another possible approach proposed by Peters in the context of RANS (Peters (1999)) is the use of a level-set approach to describe the turbulent flame front. In this methodology, the flame front is represented by an arbitrary iso-surface G_0 of a scalar field G whose evolution is described by the so-called G-equation. This equation is only valid at $G = G_0$ and is hence decoupled from other G levels. There have been various attempts to use this approach in LES of premixed turbulent combustion as well as in RANS. As the solution of the G-equation is not uniquely defined, different ways of defining the scalar G have been proposed. While Menon *et al.* (1991) and Chakravarthy *et al.* (2000)) are considering G as a progress variable (G=0 in the fresh gases, unity in the burnt gases), Peters (1999), for instance, suggests defining G as a distance function which can be described by the condition $|\nabla G(\boldsymbol{x}, t)| = 1$, where the flame front is given by $G_0 = 0$.

The latter approach seems very suitable for the description of premixed flames propagation as it allows to precisely define some important geometrical quantities such as curvature or strain. Furthermore, the numerical treatment of the step profile, inherent for the progress variable formulation, is very difficult, often leading to the introduction of diffusive terms, which incorrectly broaden the flame (Kim *et al.* (2000), Menon *et al.* (1991)).

However, we will see below that the evolution equation for G does not conserve G as a distance function, and, consequently, this property has to be enforced at each time step by a so-called reinitialization procedure. Issues related to this important aspect of the level-set method will be addressed below.

Once the proper ansatz is chosen for the scalar G, one can apply the LES formalism to the evolution equation for G. We will explain the consequent modeling of the subgrid terms arising from this process in further detail in the next section. In particular, since we are interested in performing realistic 3D simulations of reactive flows, we will try to avoid introducing any artificial diffusion term in the model that would influence the accuracy of our computation.

The model is validated using data from a turbulent Bunsen burner experiment by Chen *et al.* (1996). Numerical results from the LES are compared with measured velocity and temperature data for the cold and the reactive flow.

2. Level-set approach for premixed turbulent combustion

2.1. *The G-equation*

The level-set approach for premixed turbulent combustion is based on the assumption that the reaction zone is much smaller than the LES grid.

The flame front can then be treated as being infinitely thin and represented by a particular iso-surface of a scalar field G. This iso-surface is then convected by the velocity field $\boldsymbol{u}$ while it propagates normal to itself with the laminar burning velocity s_L. The G-field satisfies the following Hamilton-Jacobi equation known as the G-equation (Williams (1985)):

$$\rho\frac{\partial G}{\partial t} + \underbrace{\rho\boldsymbol{u}\cdot\nabla G}_{Convection} = \underbrace{\rho s_L|\nabla G|}_{Propagation} \quad . \tag{2.1}$$

In this equation the balance of diffusion and chemical reactions within the flame is represented by the laminar burning velocity. Since this quantity is only defined for the flame front, Eq. 2.1 is valid only at the $G = G_0$ level.

There are two major issues concerning the numerical treatment of Eq. 2.1: The first is the necessity to avoid the formation of cusps that naturally arise from solving Eq. 2.1 and would result in numerical problems. The second is related to the fact that, if one initially defines G as the signed distance function from the flame front by setting $|\nabla G(x; t = 0)| = 1$, this property is not naturally conserved throughout the simulation, in particular when large velocity gradients are present (Sethian (1996)).

2.2. *Regimes in premixed turbulent combustion*

Premixed combustion can be classified in different regimes as illustrated in Fig. Fig. 1 (Peters (1999), Peters (2000)).

If l_F is the laminar flame thickness, $l_\delta = \delta l_F$ the inner layer thickness, where δ can be viewed as a measure for the reaction zone thickness (see Fig. 2), η the Kolmogorov length, l the integral turbulent lengthscale, and u' the turbulent velocity fluctuation, one can define the turbulent Reynolds number Re and two different Karlovitz numbers Ka and Ka_δ as

$$\mathrm{Re} = \frac{u'l}{s_L l_F}\,, \quad \mathrm{Ka} = \frac{l_F^2}{\eta^2}\,, \quad \mathrm{Ka}_\delta = \frac{l_\delta^2}{\eta^2}\,. \tag{2.2}$$

The two regimes of particular practical interest are the corrugated flamelets regime

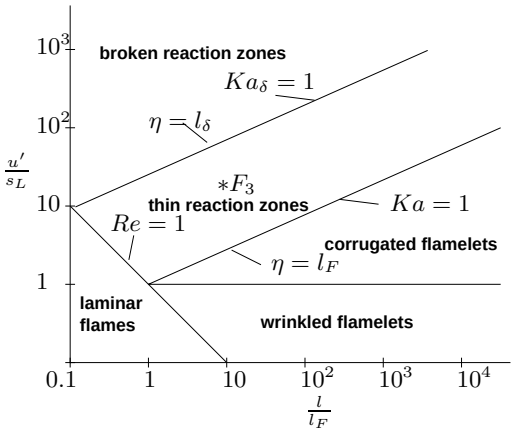

FIGURE 1. Combustion diagram.

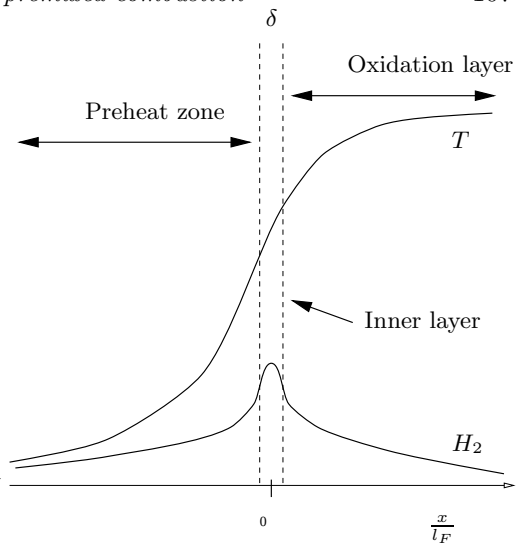

FIGURE 2. Schematic flame structure of a laminar 1-D premixed flame.

and the thin reaction zones regime and are defined by Re$>$ 1, Ka$<$ 1 and Re$>$ 1, Ka$>$ 1, $\mathrm{Ka}_\delta < 1$, respectively. In the corrugated flamelets regime, the entire flame structure including the preheat zone is smaller than the Kolmogorov scale ($l_F < \eta$). The interaction between flame and turbulence is, therefore, mainly kinematic, and the flame structure depicted in Fig. Fig. 2 remains quasi-steady. In the thin reaction zones regime, while the reaction zone is still smaller than the Kolmogorov scale, the smallest eddies can enter the pre-heat zone ($l_\delta < \eta < l_F$) and carry pre-heated fluid away to the unburnt side. This enhanced mixing is mainly responsible for the advancement of the front and a considerable thickening of the preheat zone.

In an LES framework, due to local variations in the turbulence intensity, combustion in both regimes might be present in a particular configuration. Hence, it is necessary to reflect the characteristics of both regimes in the governing equations.

A G-equation, valid in both regimes, has been derived by Peters (1999) as

$$\rho\frac{\partial G}{\partial t} + \rho\boldsymbol{u}\cdot\nabla G = \rho s_L|\nabla G| - \rho D\kappa|\nabla G|\,. \tag{2.3}$$

In this equation for both regimes, only the leading order terms which have been identified by an asymptotic analysis are included. These are the propagation term $s_L|\nabla G|$ in the corrugated flamelets regime and the curvature term $D\kappa|\nabla G|$ with D being the molecular diffusivity in the thin reaction zones regime.

2.3. *LES modeling of the filtered G-equation*

Following the classical LES filtering approach, we will decompose G and $\boldsymbol{u}$ in their Favre-filtered values ($\widetilde{G} = \overline{\rho G}/\overline{\rho}$, $\widetilde{\boldsymbol{u}} = \overline{\rho\boldsymbol{u}}/\overline{\rho}$) and subgrid fluctuations (G', $\boldsymbol{u}'$).

Applying this formalism to Eq. 2.3 leads to:

$$\underbrace{\overline{\rho}\frac{\partial\widetilde{G}}{\partial t}}_{\mathrm{I}} + \underbrace{\overline{\rho}\widetilde{\boldsymbol{u}}\cdot\nabla\widetilde{G}}_{\mathrm{II}} + \underbrace{\nabla\cdot(\overline{\rho}\widetilde{\boldsymbol{u}'G'})}_{\mathrm{III}} = \underbrace{(\rho s_L)\overline{|\nabla G|}}_{\mathrm{IV}} - \underbrace{(\rho D)\overline{\kappa|\nabla G|}}_{\mathrm{V}} \tag{2.4}$$

Terms I and II depend only on the filtered variables and do not require any modeling. Term V is proportional to the molecular diffusivity. This term can be expected to be small for the relatively large Reynolds numbers considered here and will therefore be neglected. As noted in Peters (1999) and Peters (2000), the turbulent transport term III cannot be modeled by a classical gradient transport approximation since this would result in an elliptic equation for $\widetilde{G}$ and contradict the mathematical nature of the original G-equation. Instead, according to Peters (1999), we will rewrite this term as the sum of a normal diffusion and a curvature term, where the normal diffusion term has to be included in the turbulent burning velocity and the curvature term is modeled as $\overline{\rho} D_t \widetilde{\kappa} |\nabla \widetilde{G}|$, where D_t is the turbulent eddy-diffusivity and $\widetilde{\kappa}$ the filtered front curvature. Besides the fact that this model preserves the mathematical nature of the filtered G-equation, it also has the numerical advantage that the flame front will not develop any cusps since the propagation of the flame front is now a function of its own curvature (Sethian (1996)). The turbulent eddy-diffusivity D_t can be determined using the dynamic procedure (Moin *et al.* (1991)).

The remaining term to be modeled is the turbulent propagation term IV. This term can be modeled by introducing a turbulent burning velocity s_T and enforcing that the mass flow rate through the filtered and unfiltered fronts are the same, which leads to $(\rho s_L)\overline{|\nabla G|} = \overline{\rho} s_T |\nabla \widetilde{G}|$.

Introducing the modeled terms in the filtered G-equation reads

$$\overline{\rho}\frac{\partial \widetilde{G}}{\partial t} + \overline{\rho}\widetilde{\boldsymbol{u}} \cdot \nabla \widetilde{G} = \underbrace{\overline{\rho} s_T |\nabla \widetilde{G}|}_{Propagation} - \underbrace{\overline{\rho} D_t \widetilde{\kappa} |\nabla \widetilde{G}|}_{Curvature} . \tag{2.5}$$

To close the problem, an expression for the turbulent burning velocity s_T has still to be provided.

2.4. *Modeling the turbulent burning velocity*

There have been various attempts to model the turbulent burning velocity, and this problem remains one of the most important in premixed combustion.

Most models for this quantity are generally of the form:

$$\frac{s_T}{s_L} = 1 + C \left(\frac{u'}{s_L} \right)^n , \tag{2.6}$$

where n is a value that is found to depend on the combustion regime and C is a constant.

However, as pointed out by Peters (2000), in the thin reaction zones regime the turbulent burning velocity does not only depend on the ratio of the subgrid turbulent velocity to the laminar burning velocity u'/s_L, but also on the ratio of the subgrid length scale to the flame thickness Δ/l_F. An expression for s_T, valid in both the corrugated flamelets and thin reaction zone regime, has recently been proposed in the context of RANS by Peters (1999).

For LES it can be written as

$$\frac{s_T - s_L}{s_L} = -\frac{a_4 b_3^2}{2b_1}\frac{\Delta}{l_F} + \left[\left(\frac{a_4 b_3^2}{2b_1}\frac{\Delta}{l_F} \right)^2 + a_4 b_3^2 \frac{v'\Delta}{s_L l_F} \right]^{\frac{1}{2}} , \tag{2.7}$$

where Δ is the filter size and a_4, b_1, and b_3 are constants given in Peters (2000) for RANS. For LES, a_4 can be evaluated to be $a_4 = 1.37$. The other constants might also differ from the RANS case and can be determined by DNS.

3. Reinitialization procedure

The level set method is currently a popular method to study problems in which an interface separates regions of different physical properties (Sethian (1996)). It has been discussed above that it is often useful to define G as a distance function, and since this property is not conserved by the level set equation, this condition needs to be enforced in a different way, which is commonly called reinitialization. Several methods have been derived for the reinitialization of the level set function to a signed distance (Sethian (1996), Sussman *et al.* (1999), Russo *et al.* (2000)).

3.1. *Problem formulation*

Given the numerical context of our work, we decided to use the following method, first described in Sussman *et al.* (1994) and extended by Russo *et al.* (2000). It is based on solving the following p.d.e. to a steady state:

$$\begin{cases} \dfrac{\partial \widetilde{G}}{\partial t} &= \operatorname{sgn}(\widetilde{G}^0)(1 - |\nabla \widetilde{G}|) \\ \widetilde{G}(\underline{x}, 0) &= \widetilde{G}^0(\underline{x}) \end{cases}, \tag{3.1}$$

which can be also written as:

$$\frac{\partial \widetilde{G}}{\partial t} + \operatorname{sgn}(\widetilde{G}^0)\, \underline{n} \cdot \nabla \widetilde{G} = \operatorname{sgn}(\widetilde{G}^0)\,, \tag{3.2}$$

where $\underline{n} = \nabla \widetilde{G}/|\nabla \widetilde{G}|$ is the unit normal to the level sets and $\operatorname{sgn}(\widetilde{G}^0)$ is the sign function defined by:

$$\operatorname{sgn}(\widetilde{G}^0) = \begin{cases} 1 & \text{if} \quad \widetilde{G}^0 > 0 \\ -1 & \text{if} \quad \widetilde{G}^0 < 0 \\ 0 & \text{otherwise} \end{cases} \tag{3.3}$$

Equation 3.2 clearly displays the hyperbolic nature of this equation, for which the characteristics are propagating away normally from the $\widetilde{G}^0$ level. The steady solution $\widetilde{G}$ of Eq. 3.2 obviously satisfies $|\nabla \widetilde{G}| = 1$ and has the same zero-level as $\widetilde{G}^0$. It is therefore the desired signed distance function.

3.2. *Practical implementation*

3.2.1. *Narrow band method*

Because the G-equation is only valid at the flame front, Eq. 3.1 does not need to be solved to a steady state in the entire domain, but only in a specified neighborhood of width L of the $\widetilde{G} = 0$ surface (Sussman *et al.* (1999)). This so-called narrow-band strategy is used here to limit the impact of the reinitialization procedure on the overall computational efficiency.

3.2.2. *Discretization*

Due to the hyperbolic nature of Eq. 3.1, upwind methods can be used to compute the spatial derivatives. Since all of the information propagates outward from the $\widetilde{G} = 0$ surface, boundary conditions do not have to be prescribed on the lateral boundaries of the domain. In the direct neighborhood of the front, a second order scheme is used to evaluate the signed distance function, and a first order scheme is used elsewhere.

A second order Runge-Kutta scheme is used for the time advancement. Furthermore,

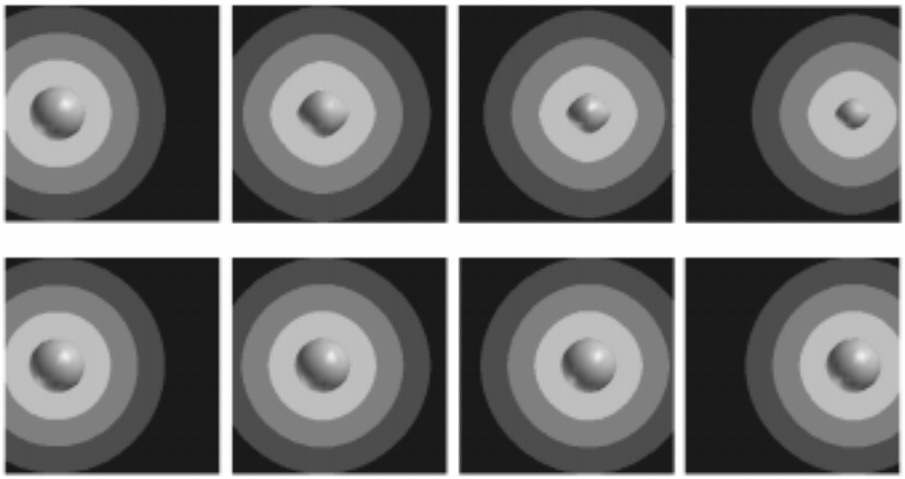

FIGURE 3. Uniform convection ($U_{conv} = 1$) of a sphere at different instants. Top: Eq. 3.1 is solved in the entire domain. Bottom: an exact method is used to determine the distance for the neighboring points of the front.

since the mesh can potentially be locally refined, we use a local time stepping strategy to alleviate the CFL condition and accelerate convergence to a steady state.

From a computational point of view, this method can easily and very efficiently be implemented in a parallel code.

3.2.3. *Sub-cell accuracy*

Some authors (Sethian (1996), Sussman *et al.* (1999), Russo *et al.* (2000)) have noticed that under certain conditions repeated reinitializations of the level set function could lead to a significant motion of the front. This is often attributed to the relative crudeness of the sign function involved in Eq. 3.1 and the fact that values of $\widetilde{G}$ at points on one side of the front are used to estimates spatial derivatives on the other side, which violates the upwind nature of the scheme (Russo *et al.* (2000)).

In a three-dimensional implementation, this can lead to a considerable loss of area of the $\widetilde{G}^0$ surface. An example of this phenomenon will be given in the next section.

In a method described by Russo *et al.* (2000), a precise estimate of the distance to the $\widetilde{G}^0$ level is computed for the points surrounding the $\widetilde{G}^0$ surface. If this is used as a boundary condition for the upwind scheme described above, the surface of the $\widetilde{G}^0$ level is essentially conserved.

We will also show that this method can initialize any given field to a signed distance function without any modifications, while preserving the shape of a prescribed interface. This is of practical importance when no *a-priori* initial location of the front can be proposed, as for instance during an ignition process.

3.3. *Validation*

3.3.1. *Uniform convection of a sphere*

In order to validate the reinitialization procedure described in the previous section, we compute the convection of a sphere in a uniform flow field.

The computational domain is a cylinder of radius $R = 1$ and length $L = 2$. It is

FIGURE 4. First-time initialization.

discretized using 32 points in the axial, radial, and azimuthal directions, respectively. The mesh is stretched in the radial direction towards the centerline to test the grid sensitivity of the algorithm.

The convection velocity of the sphere is prescribed by imposing a uniform inflow condition $U_{\text{conv}} = 1$ on the $x = 0$ boundary. All other boundaries are "free" (i.e. advective condition on $x = 2$ and $R = 1$). The $\widetilde{G}$ field is set to $\widetilde{G}(x, r, \theta; t = 0) = \sqrt{x^2 + r^2} - 0.25$.

In a first calculation, Eq. 3.1 is solved in the whole domain. Results at different instants in time are displayed on the upper part of Fig. 3. Due to the multiple reinitialization iterations, the sphere loses area and shrinks rapidly as it is convected. Also, an influence of the mesh refinement near the centerline can be observed clearly.

In the second calculation, the upwind scheme is no longer used to reinitialize the points adjacent of the $\widetilde{G}^0$ level. Instead, a direct estimate is used for the value of the signed distance function for these points. These values for $\widetilde{G}$ are then used as a boundary condition for the upwind scheme method. The resulting improvement of this method is demonstrated in the lower part of Fig. 3, where the sphere perfectly preserves its original form. Furthermore, the results do not reveal the grid sensitivity detected in the previous example.

3.3.2. *First-time initialization*

The ability of this method to initialize a given field to a signed distance function without altering the $\widetilde{G} = 0$ level is demonstrated in Fig. 4. Here, a field initially defined by $\widetilde{G}(x, r, \theta; t = 0) = f(x, r) \cdot \sqrt{x^2 + r^2} - 0.25$, where $f(x, r) = 0.1 + (x - 1)^2 + (r - 0.5)^2$ is a function designed to generate both large and small gradients near the $\widetilde{G}^0$ sphere, is reinitialized to a distance function. The $\widetilde{G}$ field is progressively set to the signed distance from the $\widetilde{G}^0$ level, while the shape of the $\widetilde{G} = 0$ level is exactly preserved.

4. Numerical simulation

4.1. *Experimental setup*

The experimental setup studied by Chen *et al.* (1996) is a stoichiometric premixed methane-air flame, stabilized by a large pilot flame. Both incoming streams, the main jet and the pilot, have the same composition. The nozzle diameter D of the main stream is 12 mm. The pilot stream issues through a perforated plate (1175 holes of 1 mm in diameter) around the central nozzle, with an outer diameter of $5.67D$. The main stream

FIGURE 5. Instantaneous flame front location and axial velocity.

is turbulent with a Reynolds number of 23486, based on the inner nozzle diameter and a bulk velocity of $U_0 = 30\,\mathrm{m/s}$.

Experimental data is available for the cold and reactive flows at downstream stations located at $x/D = 2.5$, $x/D = 4.5$, $x/D = 6.5$, and $x/D = 8.5$, respectively.

Based on the estimated characteristic length and time scale given in Chen *et al.* (1996) ($u'/S_L = 11.9$, $l/l_f = 13.7$), flame F_3 can be identified in the combustion diagram shown in Fig. 1 to be located well within the thin reaction zones regime.

4.2. *LES*

We are using the code developed at the Center for Turbulence Research by Pierce (Pierce & Moin (1998)), in which the governing equations, here the filtered zero-Mach number approximation of the Navier-Stokes equations and the filtered G-equation, are solved in cylindrical coordinates. The mesh is structured and is refined in regions of high gradients around walls and in shear layers. The numerical method consists of a conservative, second-order finite-volume scheme on a staggered grid. A second-order semi-implicit time advancement is used, which alleviates the CFL restriction in regions where the grid is refined. Details about the method can be found in Akselvoll *et al.* (1996a). The code has been thoroughly validated in various studies (see Akselvoll *et al.* (1996b), Pierce & Moin (1998)).

The computational domain extends to $20D$ downstream of the nozzle and $4D$ in the radial direction. The LES grid is $256 \times 96 \times 64$, corresponding to approximately 1.6 M cells. At the inflow boundary, instantaneous velocities extracted from a separate LES of a fully developed pipe flow are prescribed. Convective conditions (Akselvoll *et al.* (1996a)) are prescribed at the outflow boundary while traction-free conditions (Boersma *et al.* (1998)) are imposed on the lateral boundary in order to allow entrainment of fluid into the domain.

5. Results and discussion

5.1. *Instantaneous and mean flame front*

A typical example of the instantaneous flame surface is shown in Fig. 5. The presence of small regions of high negative curvature (forming cusps toward the products side) and large regions of lower positive curvature is consistent with the fact that the flame propagation is accelerated in regions of negative curvature and slowed in regions of positive

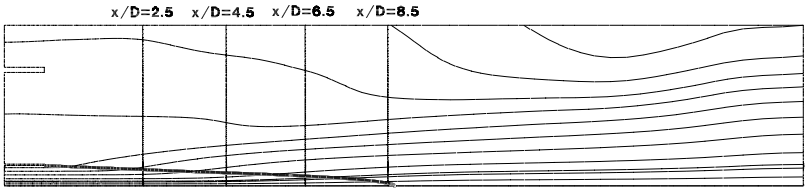

FIGURE 6. Mean flame front location and mean flow streamlines.

curvature. The acceleration of the burnt gases behind the flame front caused by the heat release is illustrated by the instantaneous field of the axial velocity given in the same figure.

This effect of dilatation induced by heat release is even more obvious in the mean quantities. The radial deflection of the mean streamlines around the time-averaged position of the turbulent flame front, which is given by a thick line, is illustrated in Fig. 6.

Due to the consumption of the unburnt mixture, the mean flame front position is converging toward the centerline. The computed time averaged axial position, where the fuel is completely consumed is at approximately $x/D = 8.6$, which is very close to the experimental value of $x/D = 8.5$ obtained by Chen *et al.* (1996). This result shows that the model for the turbulent flame speed s_T leads to a reasonable prediction of the averaged flame location.

The incoming streamlines through the upper boundary of Fig. 6 also illustrate the importance of imposing boundary conditions allowing for the entrainment of fluid into the computational domain.

5.2. *Mean temperature and axial velocity*

The mean radial profiles of temperature and axial velocity are shown in Fig. 7 for the different locations shown in Fig. 6 where $\langle\theta\rangle$ is the time-averaged non-dimensional temperature defined by $\langle\theta\rangle = (\langle T\rangle - T_u)\,/\,(T_b - T_u)$ and $\langle U\rangle$ is the time-averaged velocity normalized by the bulk velocity U_0.

Significant differences can be observed between the cold and the reactive case. In the cold flow, the mean axial velocity at the centerline is decreasing much faster than in the reactive case, where the potential core with an almost constant mean axial velocity extends to an axial position where the fuel is almost consumed. Gas expansion in the reacting jet case causes the spreading rate to be higher than for the non-reactive case. Although this effect is slightly overestimated in the computation, the overall agreement between computational results and experimental data is very reasonable.

While the evolution of the mean temperature shows generally good agreement with the experimental data, the maximum temperature close to the nozzle is overestimated in the present computation. This can be attributed to heat losses to the burner surface, which are currently being neglected.

5.3. *Turbulent kinetic energy*

The radial profiles of the mean turbulent kinetic energy k are shown in Fig. 8 for different downstream locations. For the cold flow case, the predictions of the turbulent kinetic energy are in very good agreement with experimental data for all downstream locations. The evolution of k at the centerline is found to be very different in the cold and reactive

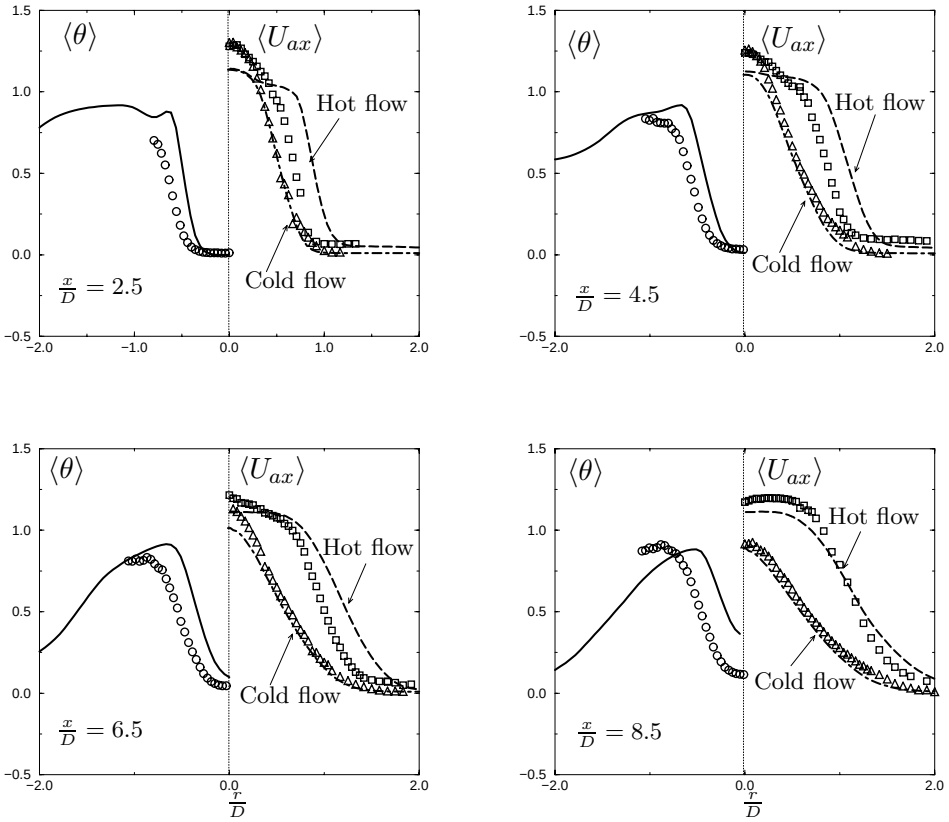

FIGURE 7. Radial profiles of the mean temperature and axial velocity at different axial positions. Symbols represent experimental data, lines are LES results.

cases. For the cold flow case, the turbulent kinetic energy is progressively increasing in downstream direction and reaches a maximum at $x/D = 8.5$, whereas it stays approximately constant for the reacting case. This result confirms that combustion strongly influences transport of turbulence toward the centerline by preventing radial mixing of turbulent kinetic energy produced within the shear layers. This important result (Chen *et al.* (1996)) is well reproduced in the simulation.

In the reactive case, the turbulent kinetic energy profile reveals two maxima, one on the burnt and one on the unburnt side of the mean flame position. At axial positions up to $x/D = 6.5$, the maximum in the unburnt is very well reproduced. Also the appearance of the second maximum on the burnt side can be observed in the predictions. However, the maximum value starts to be overpredicted at $x/D = 4.5$.

6. Conclusion and future plans

A level-set approach based on the G-equation has been formulated as a model for large-eddy simulation of turbulent premixed flames. Important issues concerning the proper implementation of this methodology in the context of LES, particularly the so called reinitialization procedure, have been discussed. To validate the model numerical

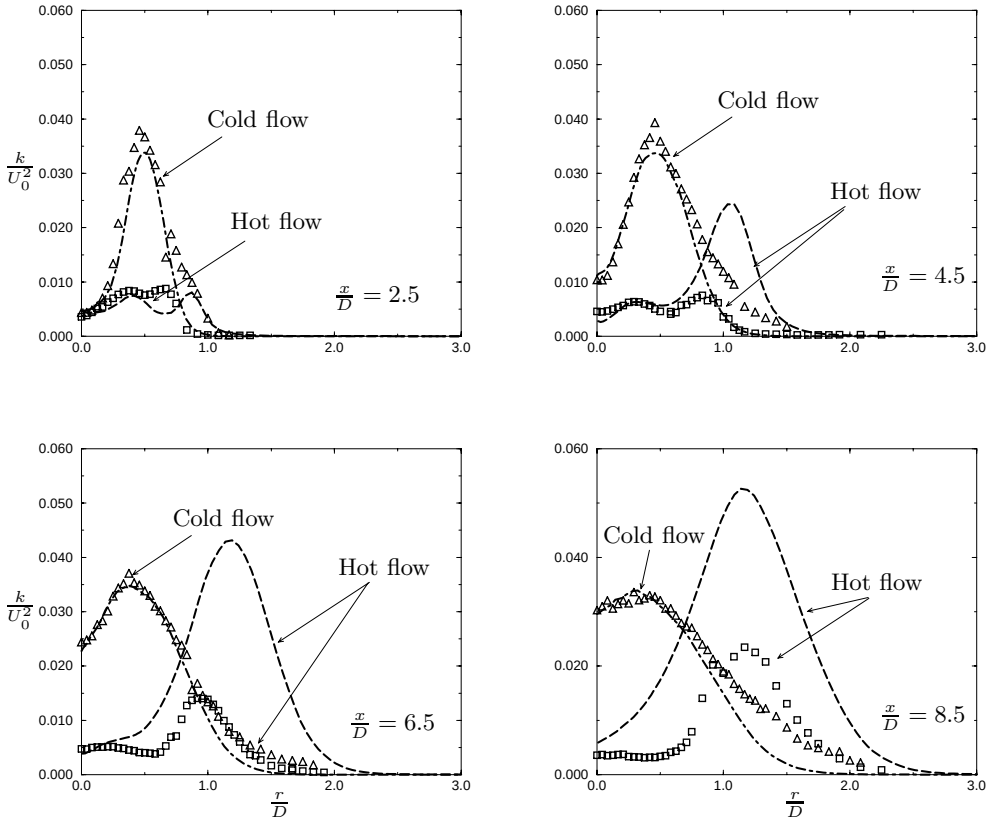

FIGURE 8. Radial profiles of the mean turbulent kinetic energy at different axial locations. Symbols represent experimental data, lines are LES results.

simulations have been performed for a turbulent methane/air Bunsen flame. The results are compared with experimental data, showing very good agreement for the mean axial velocity and turbulent kinetic energy for the cold flow case. For the reactive case mean temperature and axial velocity are essentially well predicted. However, the jet spreading rate is slightly overpredicted and the computed turbulent kinetic energy in the post-flame region is too high. In the future, a more elaborate model for the turbulent burning velocity will be applied. The resulting model will be used to study industrial-like combustor configurations.

Acknowledgments

This work was supported in part by SNECMA Motors.

REFERENCES

AKSELVOLL, K. & MOIN, P. 1996a An efficient Method for Temporal Integration of the Navier-Stokes Equations in Confined Axisymmetric Geometries. *J. Comp. Phys.* **125**, 454-463.

Akselvoll, K. & Moin, P. 1996b Large-Eddy Simulation of Turbulent Confined Coannular Jets. *J. Fluid Mech.* **315**, 387-411.

Angelberger, C., Veynante, D. & Efgelopoulos, F. 2000 LES of Chemical and Acoustic Effects on Combustion Instabilities. *Flow, Turb. and Comb.*, accepted for publication.

Boersma, B., Brethouwer, G. & Nieuwsdat, F. T. M. 1998 A Numerical Investigation on the Effect of the Inflow Conditions on the Self-Similar Region of a Round Jet. *Physics of Fluids.* **10**(4), 899-909.

Chakravarthy, V. K. & Menon, S. 2000 Large Eddy Simulation of Turbulent Premixed Flames in the Flamelet Regime. *Comb. Sci. Tech.*, accepted for publication.

Chen, Y. C., Peters N., Schneemann, G. A., Wruck, N., Renz, U. & Mansour, M. S. 1996 The Detailed Flame Structure of Highly Streched Turbulent Premixed Methane-Air Flames. *Comb. and Flames.* **107**, 233-244.

Colin, O., Ducros, F., Veynante, D. & Poinsot, T. 2000 A Thickened Flame Model for Large Eddy Simulation of Turbulent Premixed Combustion. *Physics of Fluids.* **12**(7), 1843-1863.

Kerstein, A. R., Ashurst, W. T. & Williams, F. A. 1988 Field Equation for for Interface Propagation in an Unsteady Homogeneous Flow Field. *Phys. Rev.* **A37**, 2728-2731.

Kim, W. W. & Menon, S. 2000 Numerical Modeling of Turbulent Premixed Flames in the Thin-Reaction-Zones Regimes. *Comb. Sci. Tech.* **00**, 1-32.

Menon, S., Jou, W. H. 1991 Large Eddy Simulation of Combustion Instability in an Axisymetric Ramjet Combustor. *Comb. Sci. Tech.* **75**, 53-72.

Moin, P., Squires, K., Cabot, W. & Lee, S. 1991 A Dynamic Subgrid-Scale Model for Compressible Turbulence and Scalar Transport. *Phys. Fluids A*.**3**, 2746-2757.

Peters, J. A. 1999 The Turbulent Burning Velocity for Large-Scale and Small-Scale Turbulence. *J. Fluid Mech.* **384**, 107-132.

Peters, J. A. 2000 *Turbulent Combustion.* Cambridge University Press.

Pierce, C. D. & Moin, P. 1998 Large Eddy Simulation of a Confined Jet with Swirl and Heat Release. *AIAA 98-2892.* 29^{th} AIAA Fluid Dynamic Conference.

Poinsot, T., Veynante, D. & Candel, S. 1991 Quenching Process and Premixed Combustion Diagrams. *J. Fluid Mech.* **228**, 561-606.

Russo, G. & Smereka, P. 2000 A Remark on Computing Distance Functions. *J. Comp. Phys.* **163**, 51-67 .

Sethian, J. A. 1996 *Level Set Methods: Evolving Interfaces in Geometry, Fluid Mechanics, Computer Vision and Material Science.* Cambridge University Press.

Sussman, M. Smereka, P. & Osher, S. 1994 A Level Set Method for Computing Solutions to Incompressible Two Phase Flows. *J. Comp. Phys.* **119**, 146-63.

Sussman, M. & Fatemi, E. 1999 An Efficient, Interface-Preserving Level Set Redistancing Algorithm and Its Application to Interfacial Incompressible Fluid Flow . *SIAM J. Sci. Comp.* **20**(4), 1165-1191.

Veynante, D. & Poinsot, T. 1997 Large Eddy Simulation of Combustion Instabilities in Turbulent Premixed Burners. *Annual Research Briefs*, Center for Turbulence Research, NASA Ames/Stanford Univ. 253-274.

Williams, F. A. 1985 Turbulent Combustion. *The Mathematics of Combustion*, J. Buckmaster, Ed. 97-131.